CORA Cork Open Research Archive
Cartlann Taighde Oscailte Chorcaí

Title	The stability of “Ce2O3” nanodots in ambient conditions: a study using block copolymer templated structures
Authors	Ghoshal, Tandra;Fleming, Peter G.;Holmes, Justin D.;Morris, Michael A.
Publication date	2012-09-24
Original Citation	Ghoshal, T., Fleming, P. G., Holmes, J. D. and Morris, M. A. (2012) 'The stability of “Ce2O3” nanodots in ambient conditions: a study using block copolymer templated structures', Journal of Materials Chemistry, 22(43), pp. 22949-22957. doi: 10.1039/c2jm35073d
Type of publication	Article (peer-reviewed)
Link to publisher's version	http://pubs.rsc.org/en/Content/ArticleLanding/2012/JM/c2jm35073d - 10.1039/c2jm35073d
Rights	© The Royal Society of Chemistry 2012
Download date	2026-09-08 10:00:36
Item downloaded from	https://hdl.handle.net/10468/6780

UCC
University College Cork, Ireland
Coláiste na hOllscoile Corcaigh

The stability of "Ce_2O_3" nanodots in ambient conditions: A study using block copolymer templated structures

Tandra Ghoshal[1,2,3], Peter G Fleming[1], Justin D Holmes[1,2,3], Michael A Morris[1,2,3,*]

[1]Materials research group, Department of Chemistry, University College Cork, Cork, Ireland

[2]Tyndall National Institute, Cork, Ireland

[3]Centre for Research on Adaptive Nanostructures and Nanodevices (CRANN), Trinity College Dublin, Dublin, Ireland

Table of contents:

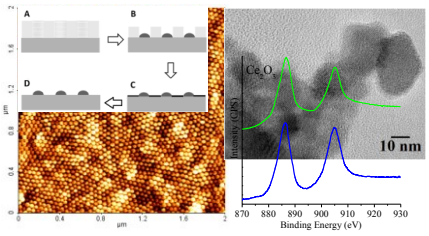

The thermal and oxidative stability of well ordered, uniform Ce_2O_3 nanodots on substrates prepared by block copolymer templating has been demonstrated in ambient conditions. The method allows easy control on the oxidation states and sizes of the nanodots as well as on their optical properties.

The stability of "Ce_2O_3" nanodots in ambient conditions: A study using block copolymer templated structures

Tandra Ghoshal[1,2,3], Peter G Fleming[1], Justin D Holmes[1,2,3], Michael A Morris[1,2,3,*]

[1]Materials research group, Department of Chemistry, University College Cork, Cork, Ireland

[2]Tyndall National Institute, Cork, Ireland

[3]Centre for Research on Adaptive Nanostructures and Nanodevices (CRANN), Trinity College Dublin, Dublin, Ireland

---

*To whom correspondence should be addressed:

Prof. Michael A. Morris

Email: m.morris@ucc.ie

Tel: 00353 21 4902180

Fax: 00353 21 4274097

The stability of reduced cerium oxide in ambient conditions is clearly demonstrated in this paper. Well-defined, crystalline, cerium oxide nanodots (predominantly Ce^{4+} or Ce^{3+} material could be selectively prepared) were defined at silicon substrate surfaces by a method of block copolymer templating. Here, selective addition of the cerium ion into one block via solvent inclusion and subsequent UV/ozone processing resulted in the formation of well-separated, size mono-dispersed, oxide nanodots having a hexagonal arrangement mimicking that of the polymer nanopattern. The size of the dots could be varied in a facile manner by controlling the metal ion content. Synthesis and processing conditions could be varied to create nanodots which have a Ce_2O_3 type composition. The stability of the sesquioxide type structure under processing (synthesis) conditions and calcination was explored. Surprisingly, the sesquioxide type structure appears to be reasonably stable in ambient conditions with little evidence for extensive oxidation until heating to temperatures above ambient. Room temperature fluorescence is supposed to originate from a distribution of surface or defect states and depends on preparation conditions.

Introduction

Ceria (CeO_2) is an important material with a large variety of applications in catalysts, fuel cell technologies, chemical-mechanical polishing for microelectronics, various phosphors, metallurgy and biomedicine.[1-6] In many of these applications it is the redox stability[7-8] and the interconversion of Ce^{3+} and Ce^{4+} that is a critical factor in defining cerium's use.[9-10] This redox chemistry is, in part, related to the similar energy of the 4f and 5d electronic states and a low potential energy barrier to electron exchange between them[11] and in principle, the different electron configurations possible can be determined by core and valence level spectroscopies.[12] The redox chemistry is dynamic and may change in response to physical parameters such as temperature, presence of other ions and the partial pressure of oxygen.[13-14] Reduction of ceria occurs through the formation of anion (oxygen) vacancy defects

(OVD). In simple terms, the presence of anion vacancies in ceria (i.e. CeO_{2-x}) are electrostatically compensated for by the existence of 'Ce^{3+}' sites although the mechanism is best described in terms of a small polaron.[15] In the Ce_2O_3 structure, the fluorite structure of ceria is modified (cubic bixbyite structure) by an ordered arrangement of the OVDs.[16-17] The importance of this redox reaction in many of ceria's applications has resulted in numerous investigations of the defect science including x-ray photoelectron spectroscopy (XPS), x-ray diffraction (XRD), electron paramagnetic resonance (EPR), scanning tunnelling microscopy (STM), Raman and neutron scattering.

Whilst much is known about ceria, little is known about the sesquioxide since it is very difficult to form via reduction and rapidly oxidizes to ceria on exposure to air. Critically, several authors have claimed that small Ce_2O_3 particles or anion vacancy containing materials can exhibit ambient stability although in many cases this is probably due to the aqueous preparative chemistry used.[18] This, however is an important point because of the implications to ceria's important applications. Definitive proof of this enhanced stability of reduced states at small dimensions is limited because of material variations, preparation dependence and sensitivity to characterisation techniques.[18]

A significant problem in studying this system has been synthesis of the particles used to study size effects. Ideally these particles should be chemically stable, uniform in size, well-dispersed and chemically/structurally controlled. Whilst it is possible to 'engineer' ideal structures via lithographic methods, the size range needed in these studies is at the limits of techniques such as e-beam, UV lithography and other methods.[19-20] A promising alternative is to utilise strictly controlled, bottom-up, self-assembly techniques such as block copolymer (BCP) microphase separation. Here, well-ordered arrangements of nanodomains of the polymer components of the BCPs can be used as an etch mask or as a nanotemplate in a deposition process.[21-22] The nanopatterned ceria nanodot materials described here were

prepared by a new methodology of selective block solvent inclusion that has been described by us elsewhere.[23-24] This technique can produce well-defined arrays of nanodots at substrates with sizes below 30 nm.

In this article, we demonstrate this method in the fabrication of an ordered pattern of cerium oxide nanoparticles on silicon wafer. It was found that the methodology could be tuned to create trivalent and tetravalent ceria structures directly without any subsequent reduction. The methodology affords an advantage over particle based studies because it avoids preparation variables and the nanostructures are considerably better defined in terms of composition, structure and size mono-dispersion. The data strongly suggest that cerium sesquioxide nanostructures can be created that are thermally and environmentally quite robust and contributes to the on-going debate about the defect chemistry of ceria in nanoparticulate form.

Experimental

A PS-b-PEO diblock copolymer was purchased from Polymer Source and used without further purification (number-average molecular weight, M_n, PS = 42 kg mol^{-1}, M_n, PEO = 11.5 kg mol^{-1}, M_w/M_n = 1.07, M_w: weight-average molecular weight). Substrates used were reclaimed 8" silicon (100) wafers with a native oxide layer. These were cleaned by ultrasonication in acetone and toluene for 30 min each and dried under a nitrogen stream. A PS-b-PEO 0.9 wt% toluene solution was aged at room temperature for 12 h and a thin film was fabricated by spin coating the polymer solution onto a silicon substrate at 3000 rpm for 30 s. The film was solvent annealed in a toluene/water (50:50, v/v) mixed vapour at 50 ^{0}C for 1 h to induce mobility and allow microphase separation to occur as described in detail elsewhere.[23-24] The resultant phase separated film was immersed in ethanol at 40^{0}C for 15h. For the fabrication of cerium oxide nanodots, cerium (III) chloride heptahydrate in ethanol was used. Different concentrations of cerium salt ethanol solution were used and these were

spin coated onto the BCP film. After drying, UV/Ozone treatment (see supporting information) was used in order to oxidize the precursor as well as to remove polymer residues. The oxidation state of the product cerium oxide was studied as a function of the UV ozone treatment time and the temperature of a subsequent anneal. For the removal of excess carbon without inducing oxidation, samples were annealed at 550^0 C for 10h under Ar/H_2 atmosphere. A horizontal quartz tube furnace was used and the sample was placed in a quartz boat inside the tube. The gas was flowed over the samples for 30 min before annealing commenced. Post-anneal sample was cooled in the gases before removal to ambient.

Surface morphologies were imaged by scanning probe microscopy (SPM, Park systems, XE-100) in tapping mode and scanning electron microscopy (SEM, FEI Company, FEG Quanta 6700). The film thicknesses were measured by optical ellipsometer (Woolam M2000). The crystalline nature and defects were revealed by transmission electron microscopy (TEM, JEOL 2100). X-Ray photoelectron spectroscopy (XPS) experiments were conducted on a Thermo K-alpha machine with an Al K_α x-ray source. All binding energies were referenced to an adventitious C 1s signal at 285.0 eV. Spectra were background subtracted using a Shirley background and the intensity envelope has been fitted with Voigt functions by tuning the binding energy, peak height and full-width half maximum value. Fourier transform infrared spectroscopy (FTIR) absorption spectra were recorded on an infrared spectrometer in ATR mode (IR 660, Varian). The photoluminescence measurements were carried out at room temperature with a fluorescence spectrophotometer (Perkin-Elmer LS 50 B).

Results and discussion

A microphase separated PS-PEO thin film prepared as detailed above by solvent annealing has a hexagonal arrangement of vertically oriented PEO cylinders in a PS matrix as described previously.[23-24] The measured average centre-to-centre cylinder spacing is 42 nm with a

PEO cylinder diameter is 19.3 nm. In order to include the metal ion in the PEO cylinders the substrate has to be 'activated' by immersion in ethanol. The activation energy involves changes in the PEO structure and is described in detail elsewhere.[23-24] Cerium oxide nanodots with the same hexagonal ordering as the BCP nanopattern were formed by simple solvent inclusion followed by a UV/ozone treatment. A well-defined cerium oxide nanodot pattern is formed after around 13 min as revealed by AFM. However, XPS data suggest that longer UV/ozone exposures are required for complete removal of the residual polymer and its degradation products (see below). Fig. 1a and 1b shows the AFM and SEM images well-ordered cerium oxide nanodots formed after UV/ozone treatment of 3h. From both the AFM and SEM images, the measured average nanodot centre-to-centre distance is 42 nm and the FFT pattern shown in the inset of Fig. 1a confirms the hexagonal ordering of the nanodots. These data are very similar to values recorded form the original BCP nanopatterns and confirm that the ceria patterns have been 'templated' via selected inclusion into the PEO cylinders of the microphase separated polymer film. With a 1 wt% cerium chloride solution the average diameter of the nanodots is 25 nm (Fig. 1a and b). The average nanodot height measured by ellipsometry is 10 nm. The nanodots formed are well-adhered to the substrate and thermally robust. Typical data is presented in the inset of Fig. 1b which shows the ordered arrangement of cerium oxide nanodots is maintained after air calcination at 1000 ^{0}C for 1 h. The only effect of heating was a reduction in the average diameter to 22 nm and height to 8 nm of the nanodots consistent with high temperature densification. The structures formed following calcination of the films formed after extended UV/ozone treatment (i.e. > 13 min) were experimentally identical to calcined films formed from a 13 min UV/ozone treatment suggesting that a 13 min UV/ozone treatment followed by calcination can be pursued for complete removal of the residual polymer as an alternative to UV/ozone treatment. Shorter UV/ozone treatments were not effective.

XPS spectroscopy was used to study the composition and oxidation state of the samples as the difference between Ce^{+3} and Ce^{+4} can be ascertained from the Ce 3d photoelectron peak XPS shape. An XPS survey spectrum of cerium oxide nanodots after a 13 minute UV/ozone treatment confirms the presence of Si, O, C and Ce. Subtracting the Si signal, the atomic concentrations of Ce, C and O were calculated and displayed in Table I for a range of sample treatments. Note, that no chlorine was observed in any data suggesting it is not contained in the final products. There is a significant carbon content following the 13 minute UV/ozone treatment and clearly originates from the residual polymer (and its' degradation products) present on the substrate. However, extended UV/ozone treatment results in reduction of the C1s peak intensity until it reaches the equivalent of about 4-6 atomic% which is typical of adventitious carbon arising from atmospheric exposure. A reduction in C1s peak intensity can also be achieved by calcination in ambient. However, a calcination to 800^0 C is required for removal of the carbon materials to a similar (Table I).

The Ce 3d photoelectron spectra of cerium compounds can be used to identify cerium valence states but are well known to be complicated because of final state effects on the hybridization of the Ce 4f orbitals with O 2p orbitals and fractional occupancy of the valence 4f orbitals.[25-26] These effects, which essentially allow electron transfer from O 2p to Ce 4f orbitals during photoemission, ensure that the Ce $3d_{5/2}$ photoelectron spectrum is complex and composed of three principle features (for each spin-orbit doublet) in the case of CeO_2 and two for Ce_2O_3.[27] In this way, a mixed valence sample can contain ten peaks altogether for overlapping Ce $3d_{5/2}$ and Ce $3d_{3/2}$ spin-orbit bands.[28] Fig. 2a shows a typical Ce 3d photoelectron spectrum exhibiting features due to trivalent and tetravalent cerium states (here, the of oxide nanodots were treated with UV/Ozone for 3 h). These features are labelled according to the original work of Burroughs et al.[29] U, $U^{//}$, $U^{///}$ and V, $V^{//}$, $V^{///}$ refer to $3d_{3/2}$ and $3d_{5/2}$ respectively and are characteristic of Ce (IV) 3d final states; while U_0, $U^{/}$ and V_0, $V^{/}$

refer to $3d_{3/2}$ and $3d_{5/2}$ respectively and are indicative of Ce(III) 3d final states. The high binding energy doublet V'''/U''' at 898.2 eV and 916.4 eV are assigned to a Ce(IV) final state of $3d^9 4f^0$ O $2p^6$. Doublets V''/U'' at 888.4 eV and 907.6 eV were attributed to the hybridization state of Ce(IV) $3d^9 4f^1$ O $2p^5$, and doublets V/U at 882.3 eV and 901.1 eV correspond to the state of Ce(IV) $3d^9 4f^2$ O $2p^4$. Doublets V'/U' and V_0/U_0 are due to a mixture of Ce(III) $3d^9 4f^2$ O $2p^4$ and Ce(III) $3d^9 4f^1$ O $2p^5$ configurations at 886 eV, 904.6eV and 880.3 eV, 899.2 eV respectively. Curve fitting of the spectra from the samples, thus, allows determination of the atomic% of Ce(III) present and this is shown in Table I for all the samples. The concentration of Ce^{3+} was calculated using the equation:

$$[Ce^{3+}] = \frac{A_{v^0} + A_{v'} + A_{u^0} + A_{u'}}{A_{v^0} + A_{v'} + A_{u^0} + A_{u'} + A_v + A_{v''} + A_{v'''} + A_u + A_{u''} + A_{u'''}} \qquad (1)$$

where, A_i is the integrated area of peak i.

Somewhat surprisingly, the analysis of the spectrum obtained for the cerium oxide nanodots treated with UV/Ozone for 13 minutes shows only doublets V'/U' and V_0/U_0 corresponding to the Ce^{+3} state (Fig. 2b(I)). This suggests that the product of reaction is Ce_2O_3 within the limit of sensitivity of the XPS technique. However, as seen above, the sample has high residual polymer content and it is unclear if the cerium is present as a pure oxide or a carbon containing phase. The O:Ce atomic ratio of 1.5:1 shown in Table I for this sample suggests that the oxide is essentially Ce_2O_3 and the carbon is largely polymer derived and not associated with cerium compound (e.g. $Ce_2(CO_3)_2$) formation. In order to affect carbon removal without extensive oxidation induced by air calcination or extended ozone treatment (see below) and, thus, produce a sesquioxide phase for comparison and investigation purposes, the sample was annealed in Ar/H_2 atmosphere at 550^0C. The Ce 3d spectrum shown in Fig. 2b(II) confirms the formation of Ce_2O_3. Subsequent quantification (Table I) in the inset of figure shows complete removal of residual polymers or carbonaceous products presumably via hydrogenation to methane and other light hydrocarbons.[30] The close

similarity of the Ce3d photoelectron peak shape for the UV/ozone treated sample before and after hydrogen treatment (Fig. 2b) confirm the formation of Ce_2O_3 in both cases. The measured O:Ce atomic ratio confirm this assignment. These data suggest that the initial product of the UV/ozone treatment is Ce_2O_3.

Fig. 3a shows an O 1s spectrum (UV/ozone for 3h) which was typical of all samples. The peaks are asymmetric and can be fitted with two Voigt functions. The major component at a binding energy 529.4 eV can be readily assigned to the lattice oxygen from the Ce-O bond but the origin of the second component at about 531.6 eV is less clear as discussed by Fleming et al recently.[31] It can derive from adsorbed carbonate or hydroxyl species and may even be associated with defect states. In the current work, we found little correspondence between the contribution of this peak to the total O1s peak area (around 20 - 25%) and the reduced state of the oxide and assume it is largely derived from adventitious adsorption.

As mentioned above, extended UV/ozone treatment times result in partial oxidation of the initial Ce^{+3} material to a Ce^{+4} oxide product as revealed by XPS. The Ce 3d spectra obtained for the cerium oxide nanodots after UV/Ozone treatments of 30 min, 1h, 2h, 3h, 4h and 5h are shown in Fig. 2c and quantified in Table I. These data show that even the longest treatment times (3-4 hours) do not result in complete oxidation and a mixed valence is observed for the samples. The data show the development of the Ce(IV) concentration in the sample and is most obvious in the growth of the feature at 920 eV. Ce^{3+} was the dominant cerium ion observed following a 30 min UV/ozone treatment and 6% of cations are found to be in the +3 state even after a 4 h treatment. To obtain a materials of essentially pure phase ceria (CeO_2) required about 5 h of UV/ozone treatment. These data do indicate unexpected resistance of the Ce(III) containing oxide nanodots to oxidation by even reactive species such as ozone. Fig. 2e shows the variation of the Ce^{+3} concentration in the nanodots with the UV/Ozone time. The measured Ce^{+3} concentration varies almost linearly with time. The time

taken to affect oxidation is very slow compared to previous measurements in ambient conditions on films and powders where high reaction rates were observed.[31-32] It might be argued that the slow reaction rates might be related to diffusion limitations but on such small samples this would seem unlikely and further, the linear dependence seen in Fig. 2e is consistent with an exposure limited process. These data therefore suggest that the dots are stable in ambient conditions and that the Ce_2O_3 in these nanodimensioned entities is much more stable than might be predicted from comparison to other material forms.

The stability of the nanodots can also be seen in analysis of the ambient oxidation which could also be used to convert the Ce_2O_3 to CeO_2. Fig. 2d shows the Ce 3d spectra of the samples following 13 minutes of UV/Ozone calcined at different temperatures between 200^0C and 800^0C. The Ce 3d data are indicative of mixed Ce(III) and Ce(IV) valence until the highest calcination temperature when the spectral envelope is reminiscent of a fully oxidised ceria material.[31] The data quantification is reported in Table I and confirms (within the level of experimental error) complete oxidation to ceria after 800^0C calcination. It should be noted that Ce3d data recorded from the hydrogen treated sample following thermal oxidation and ozone oxidation are similar to that observed from the UV/ozone 13 min only samples and data are not reproduced for clarity. However, the similarity of the data does suggest that the product of the initial UV/ozone treatment is essentially oxide rather than a carbon containing material.

Fig. 2f shows the variation of Ce^{+3} concentrations with the annealing temperature. It demonstrates that the Ce^{+3} concentration decreases with the calcination temperature. Note particularly, that a 200^0C calcination brings about only limited oxidation and a sample treated at 400^0C retains a significant Ce^{3+} component. The initial samples were stable for extended periods of weeks in ambient and together with the shape of the curve in Fig. 2f (see supporting information), the data strongly suggests that thermal oxidation from the trivalent

to tetravalent oxide is thermally activated and again confirm the analysis above that the nanodots have very enhanced stability compared to what might be expected of bulk samples.[18]

It should also be noted that these data are subject to error. Since the density of nanodots on the substrate can be estimated at about 4.2 x 10^{10} nanodots cm^{-2} it is clear that the data represent an average of a great many nanodots. Further, XPS is surface sensitive and although the dots are small, data will not refer to the total volume of the nanodot but rather a surface layer but with an inelastic mean free path of 1-2 nm, this will be a significant portion of the total dot volume. Major quantification errors arise from the curve fitting used to calculate the (3d) spectral contributions from Ce^{3+} and Ce^{4+} states. It is suggested that this is reasonably accurate as agreement is good between the stoichiometry obtained by the calculated Ce_2O_3 content and that estimated from the O:Ce atomic ratio as given by the O1s:Ce3d photoelectron peak area ratio. These are explicitly compared in table I and in generally good agreement. Indeed, the level of agreement suggests that oxide material is predominantly formed and there is little evidence for large amounts of carbonate or hydroxide being present (since O:Ce ratio would be significantly greater). This is supported by O1s shape and position and the carbon content of the oxidised materials. However, it should be stressed that because of the errors, when a material is described as Ce_2O_3 or CeO_2, this does not apply that they are non-defective only that they are close to being stoichiometric.

FTIR studies also provide additional information. A typical FTIR spectrum of the sample treated with UV/Ozone for 3h recorded in ambient is shown in Fig. 3b. All nanodot samples showed very similar data. A just observable broad band is observed between 3200-3600 cm^{-1} and corresponds to the stretching mode of hydroxyl and hydroxyl containing species. The weak intensity is consistent with adsorbed species and is consistent with the O1s photoelectron spectra. No carbonate group was observed by FTIR consistent with the low

C1s intensity reported above. The peak at 1078 cm^{-1} can be assigned to transverse optical phonon mode in -Si-O-Si-.[33]. FTIR spectra also exhibits a strong band centred at 706 cm^{-1} is due to the envelope of the phonon band of the Ce-O-Ce network.[34] In this way, the FTIR data support the suggestion that the nanodots exist as largely pure oxide after their formation in UV/ozone.

The crystalline structure of the nanodots and their interfaces with the substrate were analysed using TEM and TEM cross-sections. Such analysis is important because of the cerium oxide property dependence on crystal plane.[35-36] TEM imaging of a 1 wt% solution derived sample following calcination at 800^0C (CeO_2) is shown in Fig. 5a. The average diameter of the nanodots is 22 nm and height is 8 nm. The diameter of the nanodots is slightly reduced to that measured from the uncalcined sample (25 nm) and is most probably related to sintering. That difference is so small again supports the fact that the nanodots are essentially cerium oxide rather than a complex carbon containing species. The high resolution TEM (HRTEM) image of one of the nanodots (Fig. 5b) shows the nanodot-substrate interface. The nanodots are supported on a 1.7 nm thick amorphous native oxide at the silicon substrate surface. Parallel lattice fringes can be seen across the entire nanodot indicate that the nanodot is single crystal in nature and this was typical of the dots examined. In all cases the fringes seen were in the same direction indicating all the nanodots have the same crystallographic orientation. Unfortunately the quality of the lattice fringes from the cross-section samples was not sufficient to allow crystal structure determination.

To investigate the crystal structure and phases, nanodots on a Si substrate were scratched off by a sharp edge blade and dispersed into ethanol and then added dropwise onto a TEM grid. Fig. 5c shows the HRTEM image of a Ce_2O_3 nanodots produced by UV/ozone exposure for 13 minutes and subsequent annealing at 550^0 C under Ar/H_2 atmosphere. In comparison to the CeO_2 nanodots, described above, the sesquioxide materials are highly defective. As

well as having a polycrystalline structure, there are regions where the lattice fringes extend in slightly different directions due to defect formation.[37] Also in the micrograph there are regions of higher densities of discontinuities that can be observed and these are typical of dislocations and stacking faults consistent with the polycrystalline appearance of the nanodots. The micrographs also have dark spots and elongated dark spots which have been previously assigned to point and linear aggregations of anion vacancies in ceria.[38] This suggests that there are regions of these disordered nanodots that have a fluorite-type structure where anion vacancies are distributed in a disordered fashion. A FFT (Fast Fourier Transform) pattern obtained from the nanodot confirms the rather disordered crystalline structure present as the points observed are diffuse and low intensity. The features are labelled in the inset of Fig. 5c corresponds to hexagonal arrangement. However, as both the cubic byxbyite (111) plane and Ce_2O_3 (001) crystal planes have the hexagonal structure and their lattice constants are very close, a_0 = 0.382 nm and 0.388 nm respectively[16], it is not possible to determine the crystal structure categorically.

Fig. 5d shows the HRTEM image of a single nanodot for the sample UV/Ozone treated for 3h and which contains a majority of CeO_2. A few locations of stacking faults and defects can be seen by the discontinuity of lattice fringes or by the lack of contrast across the nanodot (marked in Fig. 5d). This suggests that the anion vacancies present (by necessity as the XPS analysis shows the presence of significant Ce^{3+}) are not arranged into an ordered superstructure within a ceria fluorite lattice structure. The indexing of the FFT pattern (inset of Fig. 5d) confirms cubic structured CeO_2 phase.[39] An HRTEM image of the sample annealed at 800^0C (CeO_2) is shown in Fig. 5e and the pseudo spherical shape of the nanodot can be clearly seen. The nanodot crystal structure is much more ordered, presumably as a result of the high temperature calcination and the sintering that occurs, and lattice planes extend across the whole sample. Similar data were recorded for all of the nanodots imaged.

The lattice planes observed are straight, parallel with no obvious discontinuities suggesting low defect concentrations. The measured interplanar spacing of 0.31 nm corresponds to the (111) reflection plane of crystalline cubic ceria.[39] The corresponding FFT pattern (inset of Figure 5e) is also in good agreement with the cubic structured ceria. The spots corresponding to interplanar distances of 0.31, 0.19, 0.16 and 0.27 nm are in good agreement with the (111), (220), (311), (200) lattice planes (respectively) of the ceria cubic fluorite structure.

Fluorescence spectra of all the samples were measured with different excitation wavelengths between 300 and 450 nm. While the fluorescence intensity changes to some extent but the band position and nature remains almost same for all excitation wavelengths between 360 and 390 nm. This indicates that the fluorescence involves the same initial and final states within this range of excitation wavelengths. This result can be explained by fast relaxation from the final state reached by photo excitation to those states from which the fluorescence originates. Comparison of fluorescence intensities provide support for the assignment of cerium oxidation states made above. Ceria is expected to have a low fluorescence intensity since the 4 eV band gap is indirect and consequently there is a low probability that radiative recombination will occur when absorption takes place.[40] In contrast, Ce_2O_3 is a semiconductor with a band gap 2.40 eV.[41] Relaxation and fluorescence yield, is increased by the possibility of 5d-4f transitions possible for Ce^{+3} ions. Thus, it is expected that as ceria is reduced to the sesquioxide, the band gap will reduce and fluorescence intensity will increase. Figs. 6a and b shows the fluorescence spectra of the UV/ozone treated and calcined samples respectively. The samples were excited with 375 nm light as this results in excitation of valence band electrons to the Ce^{3+} defect states within the ceria bandgap[40] and so the fluorescence intensity (wavelength maximum around 560 nm) is a direct measure of the Ce^{3+} content of the sample. The broad peak width indicates that fluorescence originates from a distribution of surface or defect states.[42] The intensity of the

band is observed to decrease with both the UV/ozone treatment time and the annealing temperature and is fully consistent with the oxidation of Ce^{3+} to Ce^{4+}. As might be expected from the XPS data, the high temperature calcination is most effective (compared to the extended UV/ozone treatment) in bringing about complete oxidation of the sample.

Finally, it is worth noting that the nanodot preparation technique allows control of nanodot dimension. The diameter and height of the nanodots can be varied by changing the polymer molecular weight and composition. However, a more facile approach is to vary the concentration of precursor solution which changes the size of the nanodots without changing their spacing or structural arrangement. This is illustrated in Figs. 4a, b and c, where well-ordered cerium oxide nanodot arrays can be seen. The average diameters 20, 25 and 30 nm generated from 0.5, 1 and 1.5 wt% precursor solutions. It can also be estimated from the SEM images that the height of the nanodots is increasing with higher precursor concentration. It should be noted that at cerium ion solution concentrations exceeding 2% result in the deposition of poorly defined, localised and agglomerated 3D nanoparticle structures across the substrate surface and it is clear that this concentration exceeds the amount of cation that can be inserted into the PEO cylinder.

The structural (TEM) and spectroscopic (XPS, FTIR, fluorescence) data presented here are consistent and significant in showing that ambient stable Ce_2O_3-type materials can be formed at nanodimensions. Previous work by us has shown that oxidation of reduced cerium oxides is rapid in films[32] and powders[43] and occurs at low pressures ($< 10^{-6}$ mbar) and exposures and most certainly do not survive ambient exposure with a measurable reduced component. The reason for the enhanced stability of the nanodots in reduced form could be due to several reasons but convincing arguments have been made related to the structural geometry and electrostatic interactions between ions.[44] Migani et al. have carried out theoretical work showing that a minimum in the anion vacancy formation energy (and hence increased

lifetime) exists at a small particle size. This minimum is explained by structural considerations at very small particle sizes (where lattice deformation exists because of surface tension or relaxation effects originating from repulsion of vacant orbital's at the surface[45]) ensure high vacancy formation energies, but this reduces at increasing size before increasing again as the surface moves towards the structure and electrostatics of an extended 2D surface. Inerbaev et al. have reported a similar reduction in defect formation energy also using theoretical methods.[46] Whilst theory might predict low defect formation energies in cerium oxide nanostructures and, therefore, suggest an equilibrium density of anion vacancy defects is present in nanoparticles, the number of these defects will be dependent on the oxygen pressure and the efficiency of the oxidation process.

Experimental data for ambient stable reduced nanoparticles is available but evidence is, as yet, not definitive and the work has been well reviewed recently.[18, 47] Briefly, the concept of producing anion vacancies through thermal treatments and their stability in oxidizing atmospheres has been shown for small crystallites of cubic shape.[38] Further, Tsunekawa and co-workers have led the work showing that as particle dimension reduces, there is an increased amount of anion vacancies.[48] Ivanov et al.[47] and Wu et al.[49] have suggested that there is a critical size of particle (or crystallite) where they will essentially be Ce_2O_3. However, all of these studies are subject to considerable reservations. Firstly, many of the investigative techniques can not differentiate between anion vacancy defects and the formation of Ce^{3+} states associated with e.g. hydroxyl or carbonate chemistries.[18] These states are difficult to avoid in most of the powder/colloid preparation routes used. Further, the preparation challenges limit the size monodispersity achievable and small particle aggregation is always prevalent. In this way, a complex 'composite' is normally studied and differences in structural and topographical defect densities (which have a profound effect on vacancy formation energies[44]) caused by preparation and process variables can further

complicate a proper assessment. Another well discussed problem is the sensitivity of ceria to reduction by electron and x-ray probes[50] and when critical dimensions as low as ~1 nm (or two lattice parameters) are being discussed, the propensity to effect complete e.g. x-ray reduction during study is quite high.

It is clear from this work that the methodology used can produce nanodots that are essentially Ce_2O_3 in nature and that these are stable in ambient conditions unless oxidized by ozone or via calcination. Their size, around 20 nm is considerably greater than might be expected from nanoparticles were sizes less than 10 nm are needed to see significant densities of 'reduced' components[48] and certainly, much greater than the size reported (1 – 3 nm) where complete reduction might be expected.[47, 49] Whilst, the preparative method used here avoids the problems associated with simple aqueous precipitation routes, it is suggested it has a very strong effect.

A proposed schematic of the preparation is shown in Scheme 1. The UV/ozone treatment begins to oxidize polymer and the included metal cations are immediately oxidized to oxide. It might be expected that PEO is more reactive to the treatment and decomposition is rapid leading to the formation of the oxide nanodots. During nanodot formation the products of the UV/ozone are various gaseous products (and their radicals) such as H_2, CO, CO_2, CH_4 and H_2O as well as carbonaceous residue.[51] It is the reducing nature of the products that maintain the tri-valent state. Longer UV/ozone treatments lead to removal of the PS component. It is thought that the 13 min treatment used here consists of the nanodots with a surface carbonaceous layer. On further exposure, this carbonaceous layer is removed but the reducing gases formed during polymer removal decrease so that oxidation of the sesquioxide type material can occur:

$$Ce_2O_3 + 0.5O_2 \leftrightarrow 2CeO_2 \qquad (2)$$

Here the direct oxidation by O_2 is ignored as this does not appear to occur via air exposure. Reaction (2) must be reasonably slow since much extended periods of treatment are required to bring about complete oxidation to CeO_2.

The nanodots prepared by this block copolymer inclusion technique are well adhered to the substrate, easy conversion efficiencies and uni-axial crystallographic orientation. The utility of these nanodots can be realized by means of their thermal stability since particle aggregation is common. The properties obtained from an ensemble of particles with controlled surface terminations is also highly desirable for fundamental surface science study which facilitates to understand the catalytic behaviour and further designing of better catalysts. The ambient stability of the nanodots so formed also needs to be addressed. It is clear that thermal activation is required to affect oxidation in ambient conditions. One of the models that has evolved for explaining results from nanocrystallites of cerium oxide, is that the core of a particle is CeO_2 whilst the surface layer is Ce_2O_3 like.[52] The results presented here, that surface Ce_2O_3 acts as a passivating layer preventing further oxidation of the interior and that activation is needed to allow oxygen species to migrate from the surface to the bulk to allow oxidation. This model implies that anion vacancies are intrinsically stable at the surface of the nanodots. It is suggested that these data provide strong and arguably the best evidence for the stability of defects at substrate and other supported ceria surfaces. The data suggest that reduced Ce^{3+} states may have enhanced stability compared to what might be expected.

These results may have considerable importance in terms of their application and possible use. The stability of the their low oxidation states, ease of reaction an mechanical/thermal robustness in this regular, nanopatterned, nanodot form (as compared to conventional supported catalysts) suggests they may be used in applications which require high surface activity at substrate surfaces such as antimicrobial surfaces, air pollution mitigation, sensors

and even biological assay where the ceria can be functionalised for targeted adhesion. The materials have a unique combination of ceria′s well-known redox properties and a well-defined patterned surface and this combination can enhance function through allowing access to different sites. It is clear that similar materials have been prepared before. However, the feature and pitch size is small and the preparation method can produce lithographic type structures through a very low cost method. The methodology could be introduced at relatively low capital costs and may afford significant manufacturing advantage in some of these applications.

Conclusions

The thermal and oxidative stability of Ce_2O_3-like nanodots in ambient conditions has been demonstrated. A well ordered array of cerium oxide nanodots on substrate surface was prepared via a simple and cost effective route. The nanodots have uniform size and shape and their placement mimics the original self-assembled block copolymer pattern. The Size of the nanodots can be easily tuned by changing the concentration of the precursor solutions. The crystalline nature, phases and purity of the nanodots are confirmed by XPS, FTIR and TEM analysis. A mechanism has been proposed that suggests that the stable sesquioxide type materials are produced in reducing conditions prevailing because of the reaction of the block copolymer materials used to template nanodot formation. Room temperature fluorescence is supposed to originate from a distribution of surface or defect states and depends on preparation conditions. We would also suggest that the thermal stability and strong adherence to the substrate surface may make them useful for practical applications.

Acknowledgements

The authors would like to thank Science Foundation Ireland for support of this project through the Strategic Research Cluster FORME grant and the CSET CRANN grant. The

contribution of the Foundation's Principal Investigator support is also acknowledged. We are also grateful to Dr. N Petkov (Tyndall) and Dr. Subhajit Biswas for TEM support.

References

[1] S. D. Park, J. M. Vohs and R. J. Gorte, *Nature* 2000, **404**, 265-267.

[2] G. A. Deluga, J. R. Salge, L. D. Schmidt and X. E. Verykios, *Science* 2004, **303**, 993-997.

[3] T. Masui, M. Yamamoto, T. Sakata, H. Mori and G. Adachi, *J. Mater. Chem.* 2000, **10**, 353-357.

[4] K. Otsuka, T. Ushiyama and I. Yamanaka, *Chem. Lett.* 1993, 1517-1520.

[5] M. Das, S. Patil, N. Bhargava, J. F. Kang, L. M. Riedel, S. Seal and J. J. Hickman, *Biomaterials* 2007, **28**, 1918-1925.

[6] J. M. Perez, A. Asati, S. Nath and C. Kaittanis, *Small* 2008, **4**, 552-556.

[7] F. Esch, S. Fabris, L. Zhou, T. Montini, C. Africh, P. Fornasiero, G. Comelli and R. Rosei, *Science* 2005, **309**, 752-755.

[8] T. Suzuki, I. Kosacki, H. U. Anderson and P. Colomban, *J. Am. Ceram. Soc.* 2001, **84**, 2007-2014.

[9] J. Stubenrauch and J. M. Vohs, *J. Catal.* 1996, **159**, 50-57.

[10] S. H. Overbury, D. R. Huntley, D. R. Mullins, K. S. Ailey and P. V. Radulovic, *J. Vac. Sci. Technol. A-Vac. Surf. Films* 1997, **15**, 1647-1652.

[11] A. G. Macedo, S. E. M. Fernandes, A. A. Valente, R. A. S. Ferreira, L. D. Carlos and J. Rocha, *Molecules* 2010, **15**, 747-765.

[12] S. Hufner, *Journal of Physics F-Metal Physics* 1986, **16**, L31-L34.

[13] G. S. Herman, *Surf. Sci.* 1999, **437**, 207-214.

[14] E. Mamontov, T. Egami, R. Brezny, M. Koranne and S. Tyagi, *J. Phys. Chem. B* **2000, 104**, 11110-11116.

[15] S. Deshpande, S. Patil, S. Kuchibhatla and S. Seal, *Appl. Phys. Lett.* 2005, **87**, 133113-1-3.

[16] W. D. Xiao, Q. L. Guo and E. G. Wang, *Chem. Phys. Lett.* 2003, **368**, 527-531.

[17] N. V. Skorodumova, R. Ahuja, S. I. Simak, I. A. Abrikosov, B. Johansson and B. I. Lundqvist, *Physical Review B* 2001, **64**, 115108-1-9.

[18] L. Chen, P. Fleming, V. Morris, J. D. Holmes and M. A. Morris, *J. Phys. Chem. C* 2010, **114**, 12909-12919.

[19] G. M. Wallraff and W. D. Hinsberg, *Chem. Rev.,* 1999, **99**, 1801-1821.

[20] F. Rousseaux, D. Decanini, F. Carcenac, E. Cambril, M. F. Ravet, C. Chappert, N. Bardou, B. Bartenlian and P. Veillet,. *J. Vac. Sci. Technol. B,* 1995, **13**, 2787-2791.

[21] J. Y. Cheng, , C. A. Ross, V. Z. H. Chan, E. L. Thomas, R. G. H. Lammertink and G. J. Vancso, *Adv. Mater.* 2001, **13**, 1174-1178.

[22] M. Park, C. Harrison, P. M. Chaikin, R. A. Register and D. H. Adamson, *Science* 1997, **276**, 1401-1404.

[23] T. Ghoshal, M. T. Shaw, C. Bolger, J. D. Holmes and M. A. Morris, *J. Mater. Chem.* 2012, **22**, 12083.

[24] T. Ghoshal, T. Maity, J. F. Godsell, S. Roy and M. A. Morris, *Adv. Mater.* 2012, **24**, 2390-2397.

[25] G. S. Herman, Y. J. Kim, S. A. Chambers and C. H. F. Peden, *Langmuir* 1999, **15**, 3993-3997.

[26] G. Liu, J. A. Rodriguez, J. Hrbek, J. Dvorak and C. H. F. Peden, *J. Phys. Chem. B* 2001, **105**, 7762-7770.

[27] P. W. Park and J. S. Ledford, *Langmuir* 1996, **12**, 1794-1799.

[28] M. Romeo, K. Bak, J. Elfallah, F. Lenormand and L. Hilaire, *Surf. Interface Anal.* 1993, **20**, 508-512.

[29] P. Burroughs, A. Hamnett, A. F. Orchard and G. Thornton, *J. Chem. Soc.-Dalton Trans.* 1976, 1686-1698.

[30] A. V. Talyzin, S. Luzan, I. V. Anoshkin, A. G. Nasibulin, H. Jiang, E. I. Kauppinen, V. M. Mikoushkin, V. V. Shnitov, D. E. Marchenko and D. Noreus, *ACS Nano* 2011, **5**, 5132-5140.

[31] P. Fleming, S. Ramirez, J. D. Holmes and M. A. Morris, *Chem. Phys. Lett.* 2011, **509**, 51-57.

[32] D. A. Creaser, P. G. Harrison, M. A. Morris and B. Wolfindale, *Catal. Lett.* 1994, **23**, 13-24.

[33] C. T. Kirk, *Physical Review B* 1988, **38**, 1255-1273.

[34] M. L. Dos Santos, R. C. Lima, C. S. Riccardi, R. L. Tranquilin, P. R. Bueno, J. A. Varela and E. Longo, *Mater. Lett.* 2008, **62**, 4509-4511.

[35] T. X. T. Sayle, S. C. Parker and C. R. A. Catlow, *Surf. Sci.* 1994, **316**, 329-336.

[36] D. C. Sayle, S. A. Maicaneanu and G. W. Watson, *J. Am. Chem. Soc.* 2002, **124**, 11429-11439.

[37] C. Ghica, L. C. Nistor, M. Stefan, D. Ghica, B. Mironov, S. Vizireanu, A. Moldovan and M. Dinescu, *Appl. Phys. A-Mater. Sci. Process.* 2010, **98**, 777-785.

[38] N. J. Lawrence, J. R. Brewer, L. Wang, T. S. Wu, J. Wells-Kingsbury, M. M. Ihrig, G. H. Wang, Y. L. Soo, W. N. Mei and C. L. Cheung, *Nano Lett.* 2011, **11**, 2666-2671.

[39] S. Babu, R. Thanneeru, T. Inerbaev, R. Day, A. E. Masunov, A. Schulte and S. Seal, *Nanotechnology* **2009, 20**, 085713-1-5.

[40] P. Patsalas, S. Logothetidis, L. Sygellou and S. Kennou, *Physical Review B* 2003, **68**, 035104-1-13.

[41] M. Fronzi, A. Soon, B. Delley, E. Traversa and C. Stampfl, *J. Chem. Phys.* 2009, **131**, 104701-1-17.

[42] j. Joo, T. Yu,Y. W. Kim, H. M. Park, F. X. Wu, J. Z. Zhang and T. Hyeon, *J. Am. Chem. Soc.* 2003, **125**, 6553-6557.

[43] P. G. Fleming, J. D. Holmes, D. J. Otway and M. A. Morris, *J. Solid State Chem.* 2011, **184**, 2595-2600.

[44] A. Migani, G. N. Vayssilov, S. T. Bromley, F. Illas and K. M. Neyman, *J. Mater. Chem.* 2010, **20**, 10535-10546.

[45] P. Ayyub, V. R. Palkar, S. Chattopadhyay and M. Multani, *Physical Review B* 1995, **51**, 6135-6138.

[46] T. M. Inerbaev, S. Seal and A. E. Masunov, *J. Mol. Model.* 2010, **16**, 1617-1623.

[47] V. K. Ivanov, A. E. Baranchikov, O. S. Polezhaeva, G. P. Kopitsa and Y. D. Tret'yakov, *Russ. J. Inorg. Chem.* 2010, **55**, 325-327.

[48] S. Tsunekawa, S. Ito and Y. Kawazoe, *Appl. Phys. Lett.* 2004, **85**, 3845-3847.

[49] L. J. Wu, , H. J. Wiesmann, A. R. Moodenbaugh, R. F. Klie, Y. M. Zhu, D. O. Welch and M. Suenaga, *Physical Review B* 2004, **69**, 125415-1-9.

[50] F. Zhang, P. Wang, J. Koberstein, S. Khalid and S. W. Chan, *Surf. Sci.* 2004, **563**, 74-82.

[51] J. R. Rig, Handbook of Semiconductor Wafer Cleaning Technology, Science, Technology and Applications. *Ed. W Kern, Noyes Publications*, New Jersey: **1993**.

[52] Z. H. Wu, R. E. Benfield, L. Guo, H. J. Li, Q. L. Yang, D. Grandjean, Q. S. Li and H. S. Zhu, *J. Phys.-Condes. Matter* 2001, **13**, 5269-5283.

Table-I: XPS derived chemical compositions (atomic%)

Sample	Ce^{+3} (%)	Ce (%)	O (%)	C(%)
UV/Ozone 13 minutes	100	12	18	70
UV/Ozone 13 minutes+ hydrogen annealing	100	38	58	4
UV/Ozone 30 minutes	87	18	28	54
UV/Ozone 1h	72	34	28	38
UV/Ozone 2h	44	30	53	17
UV/Ozone 3h	21	34	61	5
UV/Ozone 4h	6	33	63	4
UV/Ozone 5h	0	32	64	4
UV/Ozone 13 minutes + 200^0C	79	17	27	56
UV/Ozone 13 minutes + 400^0C	16	24	44	32
UV/Ozone 13 minutes + 600^0C	7	31	61	8
UV/Ozone 13 minutes + 800^0C	0	32	64	4

Figure Captions:

Fig. 1 (a) AFM and (b) SEM images of well-ordered cerium oxide nanodots formed after UV/ozone treatment for 3h. Insets of (a) FFT pattern reveals hexagonal ordering of the nanodots and (b) arranged nanodots after air calcination at 1000 ^{0}C for 1 h.

Fig. 2 Ce 3d spectrum of the cerium oxide nanodots treated with (a) UV/Ozone for 3h, (b)(I) UV/Ozone for 13 minutes and (II) further annealed in Ar/H_2 atmosphere at 550^{0}C, (c) UV/Ozone for different time, (d) UV/Ozone for 13 minutes and further annealed at different temperature. Inset of (b)(II) shows the survey spectrum of the corresponding sample. Variation of measured Ce^{+3} concentrations with (e) UV/Ozone time and (f) annealing temperature.

Fig. 3 (a) O 1s spectrum of cerium oxide nanodots treated with UV/Ozone for 3h. (b) FTIR spectrum of cerium oxide nanodots.

Fig. 4 Cerium oxide nanodots for different concentrations of precursor solutions (a) 0.5, (b) 1 and (c) 1.5 wt%.

Fig. 5 FIB thinned cross sectional (a) TEM image of cerium oxide nannodots annealed at 800^{0}C and (b) HRTEM image of corresponding nanodot on silicon substrate. HRTEM images of (c) Ce_2O_3 nanodots annealed at 550^0 C under Ar/H_2 atmosphere (d) Cerium oxide nanodot after UV/Ozone for 3h and (e) ceria nannodots annealed at 800^{0}C. Inset of (e) reveals corresponding lattice spacing of a single nanodot. Insets of (c), (d) and (e) shows corresponding FFT patterns.

Fig. 6 Photoluminescence spectra of cerium oxide nanodots for different (a) UV/Ozone time and (b) annealing temperatures.

Scheme 1 (A) PS-PEO thin film on substrate, (B) Cerium ion inclusion after spin coating, (C) UV/Ozone treatment for shorter time and (D) UV/Ozone treatment for longer time or after annealing.

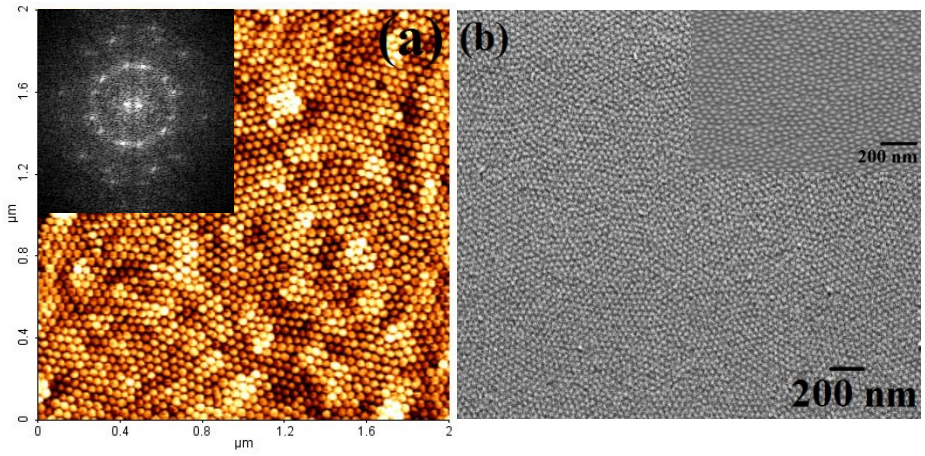

Fig. 1

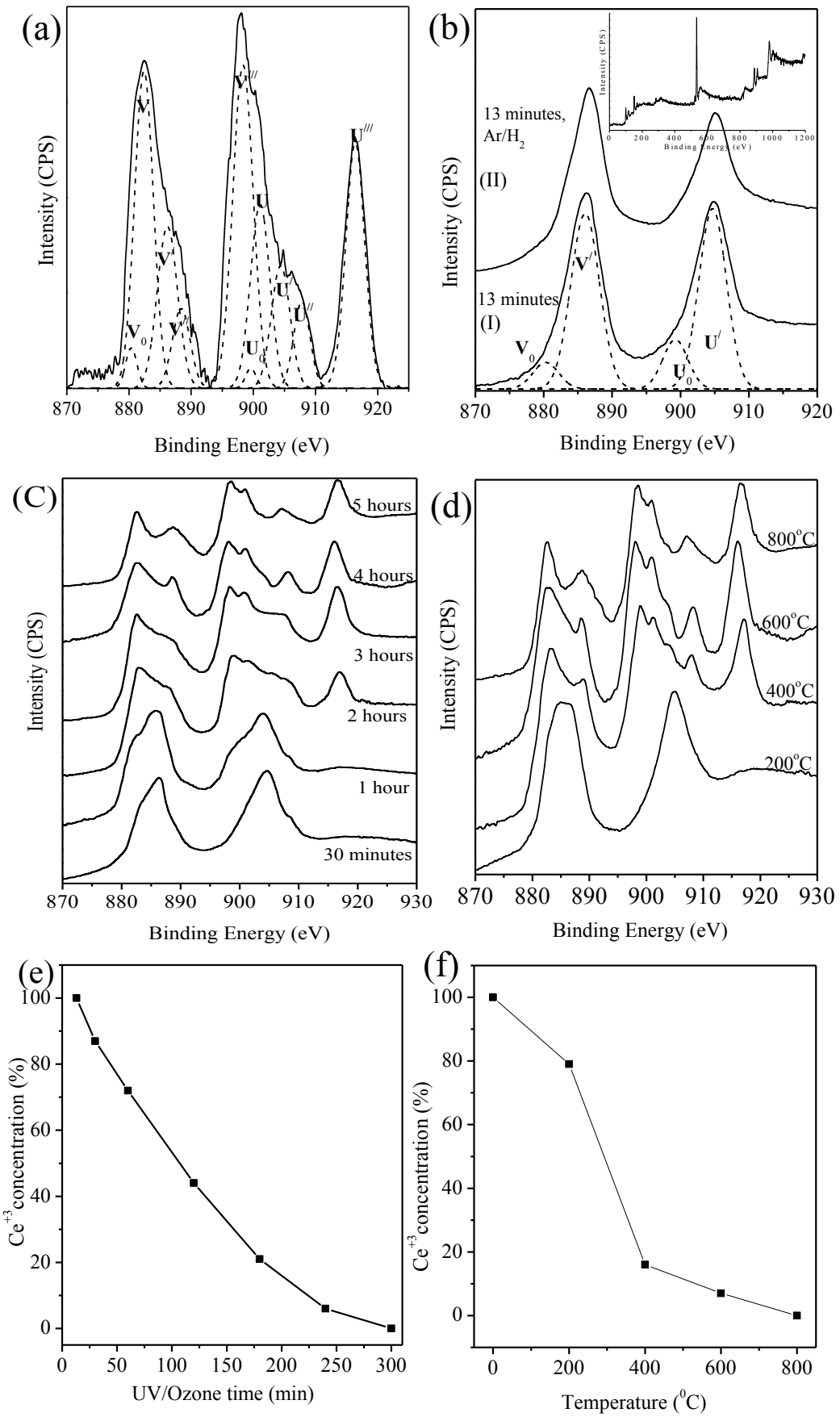
(a)
Intensity (CPS)
Binding Energy (eV)
(b)
13 minutes, Ar/H2
(II)
13 minutes
(I)
Intensity (CPS)
Binding Energy (eV)
(C)
5 hours
4 hours
3 hours
2 hours
1 hour
30 minutes
Intensity (CPS)
Binding Energy (eV)
(d)
800°C
600°C
400°C
200°C
Intensity (CPS)
Binding Energy (eV)
(e)
Ce+3 concentration (%)
UV/Ozone time (min)
(f)
Ce+3 concentration (%)
Temperature (°C)

Fig. 2

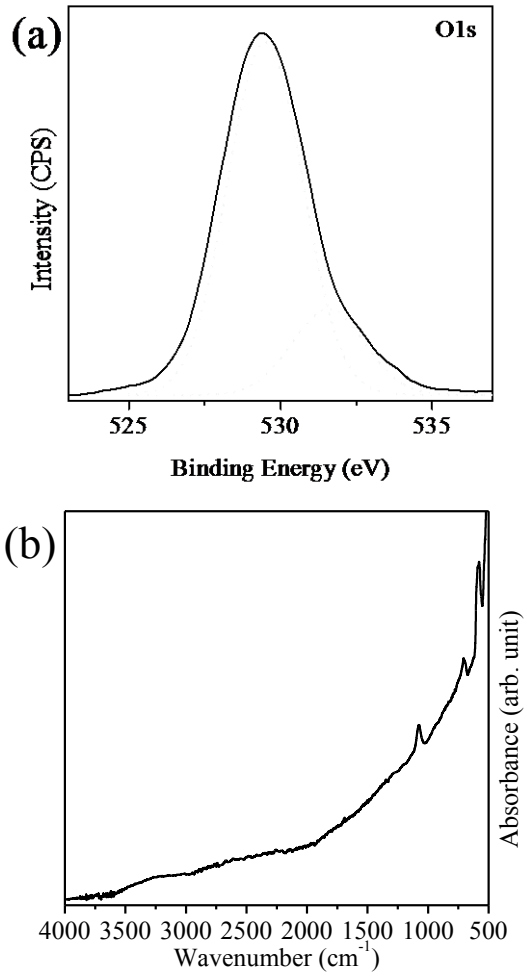
(a)
O1s
Intensity (CPS)
525
530
535
Binding Energy (eV)
(b)
Absorbance (arb. unit)
4000 3500 3000 2500 2000 1500 1000 500
Wavenumber (cm-1)

Fig. 3

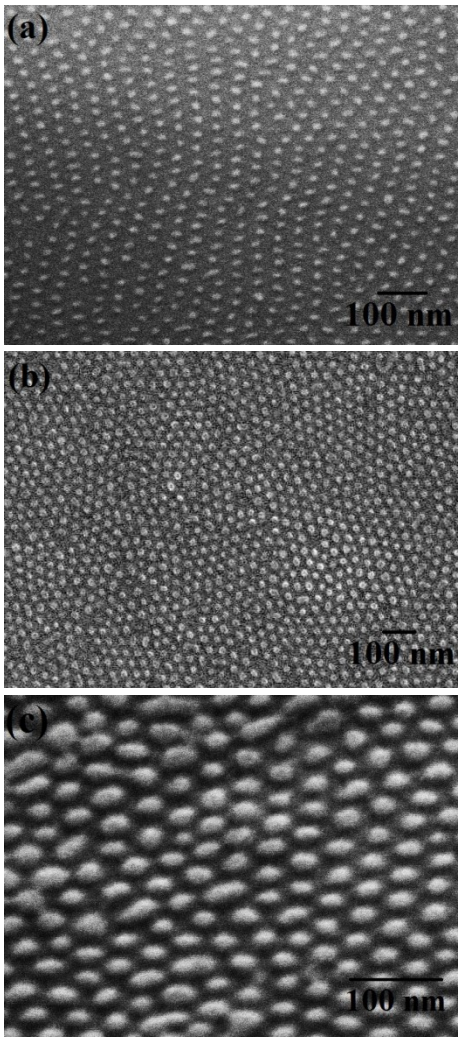

Fig. 4

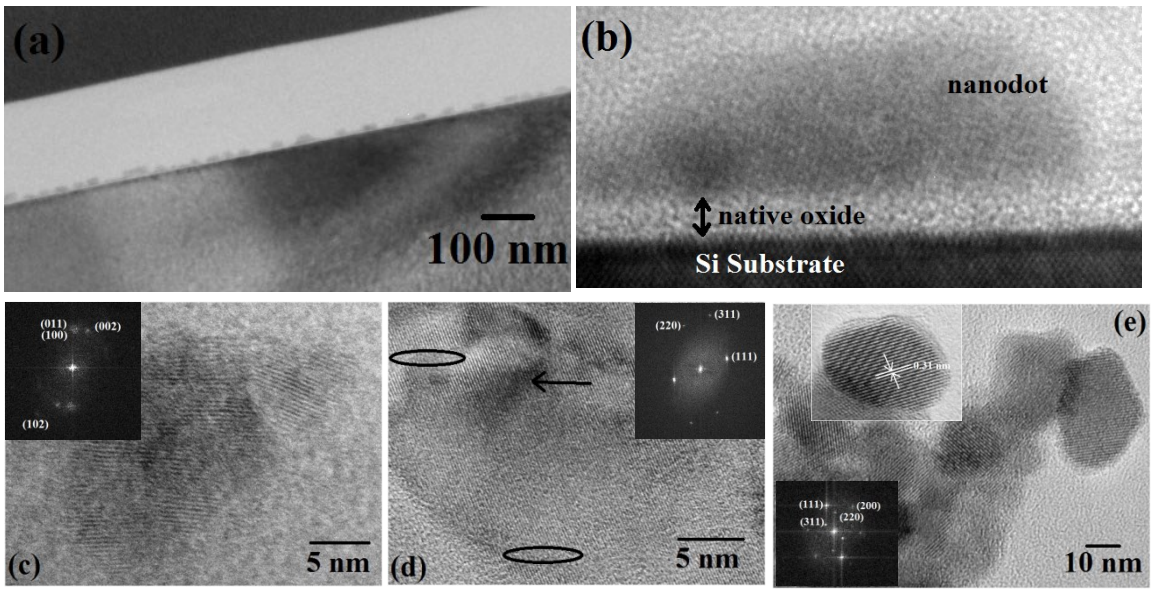
(a)
100 nm
(b)
nanodot
native oxide
Si Substrate
(011)
(100)
(002)
(102)
(c)
5 nm
(220)
(311)
(111)
(d)
5 nm
(e)
0.31 nm
(111)
(200)
(311)
(220)
10 nm

Fig. 5

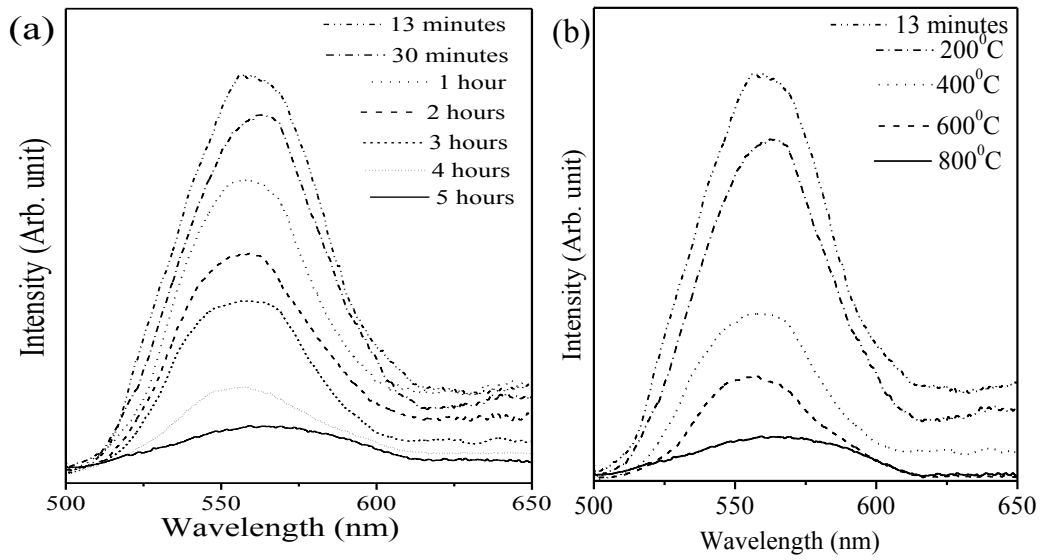
(a)
13 minutes
30 minutes
1 hour
2 hours
3 hours
4 hours
5 hours
Intensity (Arb. unit)
500
550
600
650
Wavelength (nm)
(b)
13 minutes
200^{0}C
400^{0}C
600^{0}C
800^{0}C
Intensity (Arb. unit)
500
550
600
650
Wavelength (nm)

Fig. 6

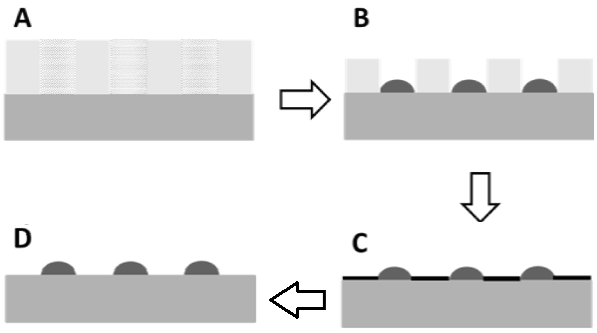

Scheme 1

Supporting Information

Details of UV/Ozone treatment: In the UV/Ozone treatment, ozone, an active oxidizing agent, is generated in situ from atmospheric oxygen by exposure to 185 nm UV light. The ozone produced subsequently photo dissociates into molecular oxygen and atomic oxygen upon exposure to 254 nm light. The latter specie reacts with the polymer to form free radicals and activated species that eventually remove organic portions of the polymer in the form of carbon dioxide, water, and a small amount of volatile organic compounds.

Stability of the samples calcined at lower temperatures in ambient:

It is observed that the Ce^{+3} concentration decreases with the calcination temperature. Calcination at 200^0C causes limited oxidation and also calcinations at 400^0C retains a significant Ce^{3+} component. It was also observed that the samples were stable for extended periods of weeks in ambient. Fig. 1a and b shows the high resolution Ce 3d and photoluminescence spectra of the samples calcined at 200^0C and 400^0C and further sustained for 30 days in ambient. The spectra strongly suggest that the samples were reasonably stable at ambient atmosphere.
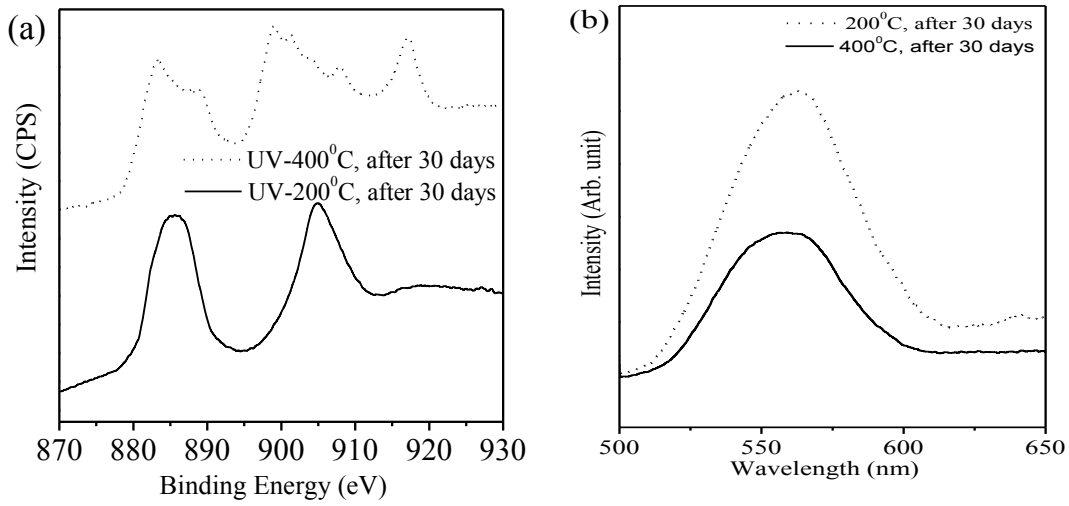
Fig.1: (a) XPS Ce 3d and (b) photoluminescence spectra of the samples calcined at 200^0C and 400^0C and further sustained for 30 days in ambient.